

Optical-cavity tests of higher-order Lorentz violation

Matthew Mewes

*Department of Physics and Astronomy, Swarthmore College,
Swarthmore, Pennsylvania 19081, USA*

The effects of Lorentz-violating operators of nonrenormalizable dimension in optical resonant cavities are studied. Optical-frequency experiments are shown to provide sensitivity to nondispersive nonbirefringent violations that is many orders of magnitude beyond current constraints from microwave cavities. Existing experiments based on Fabry-Pérot and ring resonators are considered as illustrations.

I. INTRODUCTION

Lorentz invariance is a cornerstone of modern physics. However, the possibility that Planck-scale physics may give rise to minute defects in this fundamental principle [1] has motivated numerous experimental tests of Lorentz symmetry. Searches for Lorentz violation have been performed in many different systems, including those involving photons [2]. Among these are modern versions of the classic Michelson-Morley experiment [3]. The contemporary experiments are based on electromagnetic resonant cavities and provide extreme sensitivity to potential Lorentz violation [4–10].

A theoretical framework known as the Standard-Model Extension (SME) provides a general field-theoretic description of Lorentz and CPT violation at attainable energies [11]. The SME aids in the identification of experimental signatures and in the comparison of different measurements. Many tests of Lorentz and CPT invariance have focused on the minimal Standard-Model Extension (mSME), which restricts attention to Lorentz-violating operators of renormalizable dimension in flat spacetime. However, recent studies have extended the SME formalism to Lorentz violation involving curved spacetime [12, 13] and nonrenormalizable operators [10, 14–18]. This work examines the effects of higher-order nonrenormalizable electromagnetic operators in optical resonant-cavity experiments [15].

The Lorentz-violating terms in the photon sector of SME can be classified according to various properties, such as the dimension d of the operator. The renormalizable operators of the mSME have dimensions $d = 3, 4$, while operators of higher dimension, $d \geq 5$, are nonrenormalizable. The odd-dimensional operators break CPT, in addition to breaking Lorentz invariance.

It is also useful to split the set of Lorentz-violating operators into those that affect the vacuum propagation of light and those that do not, at leading order. For example, some operators result in vacuum birefringence, which causes polarization to change as light propagates through empty space [14, 15, 19, 20]. Lorentz violation can also lead to dispersion, giving rise to energy-dependent propagation speeds [14–16]. Both these effects can be tested to very high precision using light from astrophysical sources, where the tiny effects of Lorentz violation are enhanced by the cosmological distances involved, but not all forms

of Lorentz violation result in leading-order birefringence or dispersion. The nonbirefringent nondispersive operators are comparatively difficult to detect, since they have little effect on light propagating *in vacuo*. They do, however, affect electromagnetic resonances in cavities. Cavity-based experiments thus provide a class of Lorentz-invariance tests that complement astrophysical tests.

The nonbirefringent nondispersive violations are controlled by the set of camouflage coefficients [15] and are the main focus of this work. Camouflage coefficients exist for even dimensions $d \geq 4$ and are invariant under CPT. Here, we examine the prospect of measuring higher-dimensional ($d \geq 6$) camouflage coefficients using optical cavities. At present, the only bounds on these coefficients are from a microwave-cavity experiment, which placed constraints on combinations of $d = 6$ and $d = 8$ coefficients [10].

The sensitivity to the various camouflage coefficients is largely determined by the frequency and geometry of the modes excited in a cavity experiment. For example, many experiments utilize cavities that are symmetric under a parity transformation. These have been found to provide direct access to parity-even anisotropic coefficients in the SME through direction-dependent resonant frequencies. In contrast, the effects from parity-odd and isotropic coefficients only contribute through boost violations. As a result, they enter in conjunction with the boost velocity β for parity-odd violations and the velocity-squared β^2 for isotropic violations. The relevant boost speeds are normally those from the rotational and orbital motion of the Earth, $\beta \lesssim 10^{-4}$, leading to suppressed sensitivities to parity-odd and isotropic violations. This suppression may be overcome by use of parity-breaking interferometers and resonators [9, 21–23]. Other techniques for testing these violations include those involving static fields [24], accelerators [25], and Čerenkov radiation [26], among others [27].

There are several major advantages to optical experiments. First, to a good approximation, the resonances can be taken as plane waves. As demonstrated below, this yields analytic expressions for the frequency shifts, where microwave cavities typically require numerical calculations. Second, parity-violating cavities, such as ring resonators, are comparatively easy to construct at optical frequencies. Finally, in general, the sensitivity to

higher-order coefficients grows with frequency as ω^{d-4} . This implies the potential for improved sensitivities by approximately a factor $10^{4(d-4)}$ over microwave experiments. We therefore expect improvements in sensitivity of roughly eight orders of magnitude for $d = 6$ and sixteen orders of magnitude for $d = 8$.

This paper is organized as follows. In Sec. II, we discuss some basic theory that is common to all optical-cavity experiments. The sections that follow provide analyses of several recent experiments [7–9], as illustrations. In Sec. III, we derive the sensitivity of crossed Fabry-Pérot cavities to parity-even Lorentz violations. A parity-odd experiment based on a ring resonator is considered in Sec. IV.

II. BASIC THEORY

In this section, we establish the basic theory behind most cavity-based experiments. A more detailed explanation of the nonrenormalizable terms considered here can be found in Ref. [15]. Here we summarize the parts that are relevant to optical experiments.

The basic idea behind a typical resonator experiment is to look for a shift in resonant frequency due to Lorentz violation [19]. In general, this shift will be frame dependent, leading to variations in frequency with changes in cavity orientation or speed. This work focuses on changes in orientation due to active rotations of the cavity in the laboratory and to the rotation of the Earth throughout the day.

We begin by focussing on nonbirefringent Lorentz violations, which are characterized by coefficients $(c_F^{(d)})_{n,jm}^{(0E)}$ in the SME. These coefficients are associated with even-dimensional operators, $d = \text{even} \geq 4$. The n index controls the frequency/wavelength dependence and is limited by $0 \leq n \leq d - 2$. Rotational properties are determined by the usual angular momentum indices j and m , where $j = n, n - 2, \dots, \geq 0$ and $|m| \leq j$. The shift in resonant frequency due to nonbirefringent terms in the SME takes the form

$$\frac{\delta\nu}{\nu} = \sum_{dn,jmm'} \mathcal{M}_{(c_F)n,jm}^{(d)\text{lab}} e^{im\phi + im'\omega_\oplus T_\oplus} d_{mm'}^{(j)}(-\chi) (c_F^{(d)})_{n,jm'}^{(0E)}. \quad (1)$$

The $\mathcal{M}_{(c_F)n,jm}^{(d)\text{lab}}$ are experiment-dependent factors that determine the sensitivity of the resonator to Lorentz violation.

It is important to specify the frame in which various

quantities are defined. By convention we define the coefficients for Lorentz violation $(c_F^{(d)})_{n,jm}^{(0E)}$ in the Sun-centered frame defined in Ref. [2]. This frame is inertial to a very good approximation, so the coefficients in this frame are constant. We could, in principle, calculate the $\mathcal{M}_{(c_F)n,jm}^{(d)}$ matrices in this same frame, but they would then vary in time. This is because they take the orientation of the cavity into account, and the orientation relative to the Sun frame changes with time, giving rise to a varying $\mathcal{M}_{(c_F)n,jm}^{(d)}$ matrix.

Alternatively, we can account for the change in orientation by adopting a rotating laboratory frame within which the cavity is stationary. In this frame, the $\mathcal{M}_{(c_F)n,jm}^{(d)\text{lab}}$ are constants. The changes in orientation are then incorporated through the rotation that relates the two frames. This rotation takes the form of the $e^{im\phi + im'\omega_\oplus T_\oplus} d_{mm'}^{(j)}(-\chi)$ factor in the frequency shift.

The $d_{mm'}^{(j)}$ are little Wigner matrices, and χ is the colatitude of the laboratory. By convention, the laboratory-frame z axis is vertical. The angle ϕ is the angle between the laboratory-frame x axis and south. The angle $\omega_\oplus T_\oplus$ is the right ascension of the local zenith, where $\omega_\oplus \simeq 2\pi/(23 \text{ hr } 56 \text{ min})$ is the Earth's sidereal rotation rate. Many experiments place the cavities on turntables. In this case, we may write $\phi = \omega_{\text{tt}} T_{\text{tt}}$, where ω_{tt} is the turntable rotation rate.

The $\mathcal{M}_{(c_F)n,jm}^{(d)\text{lab}}$ constants can be found perturbatively using the conventional electric field \mathbf{E} for the resonant mode being studied. To avoid divergences in the calculation that stem from discontinuities at the boundary of the cavity, we must also define a smoothed field $\underline{\mathbf{E}}$, which matches \mathbf{E} inside the resonator, but extends smoothly to the outside region. Switching to momentum space, the fields contribute to $\mathcal{M}_{(c_F)n,jm}^{(d)\text{lab}}$ through the spin-weighted Stokes combinations

$$\begin{aligned} \underline{s}^0 &= (E_+)^* \underline{E}_+ + (E_-)^* \underline{E}_- , \\ \underline{s}_{(\pm 2)} &= 2(E_\pm)^* \underline{E}_\mp , \end{aligned} \quad (2)$$

where $E_\pm = \mathbf{E} \cdot (\hat{\boldsymbol{\theta}} \pm i\hat{\boldsymbol{\varphi}})/\sqrt{2}$ and $\underline{E}_\pm = \underline{\mathbf{E}} \cdot (\hat{\boldsymbol{\theta}} \pm i\hat{\boldsymbol{\varphi}})/\sqrt{2}$. Here, $\hat{\boldsymbol{\theta}}$ and $\hat{\boldsymbol{\varphi}}$ are the usual unit vectors associated with the polar angle θ and azimuthal angle φ . In momentum space, θ is the angle between the momentum \mathbf{p} and the z axis, while φ is the angle between \mathbf{p} and the x - z plane.

For optical resonators, the $\mathcal{M}_{(c_F)n,jm}^{(d)}$ matrix elements are given by [15]

$$\begin{aligned} \mathcal{M}_{(c_F)n,jm}^{(d)} &= \frac{\omega^{d-4-n}}{4\langle U \rangle} \int d^3p p^{n-2} \left[\frac{1}{4}(\omega^2 - p^2) \sqrt{\frac{(j+2)!}{(j-2)!}} (+2Y_{jm}(\hat{\mathbf{p}}) \underline{s}_{(+2)}(\mathbf{p}) + -2Y_{jm}(\hat{\mathbf{p}}) \underline{s}_{(-2)}(\mathbf{p})) \right. \\ &\quad \left. + \left((n - \frac{j(j+1)}{2})(\omega^2 - p^2) - (d-2-n)(d-3-3n)p^2 - n(n-1)p^2 \right) {}_0Y_{jm}(\hat{\mathbf{p}}) \underline{s}^0(\mathbf{p}) \right] , \end{aligned} \quad (3)$$

where ${}_sY_{jm}$ are spin-weighted spherical harmonics and $\langle U \rangle = \frac{1}{4} \int d^3p (\mathbf{E}^* \cdot \mathbf{D} + \mathbf{B}^* \cdot \mathbf{H})$ is the time-averaged energy in the cavity. In general, there are additional terms in $\mathcal{M}_{(c_F)njm}^{(d)}$ that arise from longitudinal polarization. These, however, do not contribute in optical resonators where the fields can be approximated as transverse-polarized plane waves. We illustrate how to use Eq. (3) to get the laboratory-frame $\mathcal{M}_{(c_F)njm}^{(d)\text{lab}}$ constants in the following sections.

In practice, experiments search for the frequency shift by comparing the resonances of two different cavities or modes. The beat frequency between the two modes is then analyzed for variations at the sidereal and turntable rotation rates. The beats will depend on $\Delta\mathcal{M}_{(c_F)njm}^{(d)\text{lab}}$, the difference between the $\mathcal{M}_{(c_F)njm}^{(d)\text{lab}}$ constants for the two modes. It is convenient to write the beat frequency as

$$\frac{\nu_{\text{beat}}}{\nu} = \sum_{dnjmm'} A_{mm'} e^{im\phi + im'\omega_{\oplus}T_{\oplus}}, \quad (4)$$

where

$$A_{mm'} = \sum_{dnj} \Delta\mathcal{M}_{(c_F)njm}^{(d)\text{lab}} d_{mm'}^{(j)}(-\chi)(c_F^{(d)})_{njm'}^{(0E)}. \quad (5)$$

The $A_{mm'}$ factors are linear combinations of coefficients for Lorentz violation, which satisfy $A_{mm'}^* = A_{(-m)(-m')}$. They represent the complex combinations of coefficients a given experimental configuration can access.

Two basic strategies can be used to extract constraints on coefficients for Lorentz violation. The first is to search directly for variations at rates $\omega_{mm'} = m\omega_{\text{tt}} + m'\omega_{\oplus}$. However, since ω_{\oplus} is typically much smaller than ω_{tt} , the frequencies $\omega_{mm'}$ are closely spaced around the harmonics of the turntable rotation frequency, making it difficult to discriminate many of the variations in the beat frequency.

The second strategy for analysis relies on the fact that the sidereal variations ($m'\omega_{\oplus}$) can be viewed as slow modulations of the amplitudes of the harmonics of the turntable frequency. That is, we write [10]

$$\frac{\nu_{\text{beat}}}{\nu} = \sum_{m \geq 0} [C_m(T_{\oplus}) \cos(m\phi) + S_m(T_{\oplus}) \sin(m\phi)], \quad (6)$$

where

$$\begin{aligned} C_m(T) &= \sum_{m' \geq 0} [C_{mm'}^C \cos(m'\omega_{\oplus}T) + C_{mm'}^S \sin(m'\omega_{\oplus}T)], \\ S_m(T) &= \sum_{m' \geq 0} [S_{mm'}^C \cos(m'\omega_{\oplus}T) + S_{mm'}^S \sin(m'\omega_{\oplus}T)]. \end{aligned} \quad (7)$$

The sidereal amplitudes are given by

$$\begin{aligned} C_{mm'}^C &= 2\eta_m\eta_{m'} \text{Re}[A_{mm'} + A_{m(-m')}] , \\ C_{mm'}^S &= -2\eta_m \text{Im}[A_{mm'} - A_{m(-m')}] , \\ S_{mm'}^C &= -2\eta_{m'} \text{Im}[A_{mm'} + A_{m(-m')}] , \\ S_{mm'}^S &= -2\text{Re}[A_{mm'} - A_{m(-m')}] , \end{aligned} \quad (8)$$

where $\eta_0 = 1/2$, and $\eta_m = 1$ when $m \neq 0$. Eq. (8) gives real linear combinations of coefficients for Lorentz violation that the experiment can measure. The theoretical analysis is then reduced to finding these combinations in terms of the $(c_F^{(d)})_{njm}^{(0E)}$ coefficients.

The above gives the sensitivity of a cavity experiment to the nonbirefringent Lorentz-violating operators of the SME. However, many of the $(c_F^{(d)})_{njm}^{(0E)}$ coefficients lead to vacuum dispersion. To get the sensitivity to the camouflage coefficients, we now restrict attention to the subset of the $(c_F^{(d)})_{njm}^{(0E)}$ coefficients that are nondispersive. These are denoted by $(\bar{c}_F^{(d)})_{njm}^{(0E)}$. Setting all other coefficients to zero, the camouflage coefficients are related to $(c_F^{(d)})_{njm}^{(0E)}$ through

$$(c_F^{(d)})_{njm}^{(0E)} = (\bar{c}_F^{(d)})_{njm}^{(0E)} - (\bar{c}_F^{(d)})_{(n-2)jm}^{(0E)}. \quad (9)$$

They are nonzero for index values in the ranges $d = \text{even} \geq 4$, $0 \leq n \leq d-4$, and $j = n, n-2, \dots, \geq 0$. We can find the sensitivity to the camouflage coefficients by simply replacing $(c_F^{(d)})_{njm}^{(0E)}$ with $(\bar{c}_F^{(d)})_{njm}^{(0E)}$ and $\mathcal{M}_{(c_F)njm}^{(d)}$ with

$$\mathcal{M}_{(\bar{c}_F)njm}^{(d)} = \mathcal{M}_{(c_F)njm}^{(d)} - \mathcal{M}_{(c_F)(n+2)jm}^{(d)} \quad (10)$$

in the beat frequency.

The dimension-four operators for Lorentz violation provide one more class of coefficients that are nondispersive. This special case exists because none of the $d = 4$ operators lead to energy-dependant velocities. Consequently, the portion of $(c_F^{(d)})_{njm}^{(0E)}$ that is dispersive for $d > 4$ is not dispersive for $d = 4$.

There exists an alternative equivalent representation of these $d = 4$ coefficients, which naturally arises in the analysis of plane waves. Denoted by $c_{(I)jm}^{(4)}$, they are related to the $(c_F^{(4)})_{njm}^{(0E)}$ coefficients through

$$\begin{aligned} (c_F^{(4)})_{200}^{(0E)} &= \frac{1}{3}(c_F^{(4)})_{000}^{(0E)} = \frac{1}{4}c_{(I)00}^{(4)}, \\ (c_F^{(4)})_{11m}^{(0E)} &= -2c_{(I)1m}^{(4)}, \\ (c_F^{(4)})_{22m}^{(0E)} &= c_{(I)2m}^{(4)}. \end{aligned} \quad (11)$$

Sensitivity to this set of coefficients can be found by replacing $(c_F^{(d)})_{njm}^{(0E)}$ with $c_{(I)jm}^{(d)}$ and $\mathcal{M}_{(c_F)njm}^{(d)}$ with $\mathcal{M}_{(I)jm}^{(d)}$ in the beat frequency. The relation between the $\mathcal{M}_{(c_F)njm}^{(4)}$ and $\mathcal{M}_{(I)jm}^{(4)}$ matrix elements is

$$\begin{aligned} \mathcal{M}_{(I)00}^{(4)} &= \frac{3}{4}\mathcal{M}_{(c_F)000}^{(4)} + \frac{1}{4}\mathcal{M}_{(c_F)200}^{(4)}, \\ \mathcal{M}_{(I)1m}^{(4)} &= -2\mathcal{M}_{(c_F)11m}^{(4)}, \\ \mathcal{M}_{(I)2m}^{(4)} &= \mathcal{M}_{(c_F)22m}^{(4)}. \end{aligned} \quad (12)$$

This completes our discussion of the basic theory. We consider two optical-cavity experiments in the following sections, as illustrations.

III. FABRY-PÉROT CAVITY

To find the effects of the camouflage coefficients for Lorentz violation in Fabry-Pérot cavities, we model the field inside the cavity as a linearly polarized standing wave. We start by defining a reference frame with its z axis along the cavity axis and the polarization in the y direction. The nonzero field components can then be taken as $E_y(\mathbf{x}) = \mathcal{E}\rho(\mathbf{x})\sin kz$, where we define a profile function with $\rho = 1$ inside the beam and $\rho = 0$ outside the beam. For the smoothed field, we simply extend the standing wave to infinity, giving $\underline{E}_y(\mathbf{x}) = \mathcal{E}\sin kz$ everywhere.

The next step in the calculation is to find the \mathbf{p} -space versions of the fields, $\mathbf{E}(\mathbf{p})$ and $\underline{\mathbf{E}}(\mathbf{p})$. The fact that

$\underline{E}_y(\mathbf{x})$ is a standing plane wave implies $\underline{E}_y(\mathbf{p})$ contains contributions from $\mathbf{p} = \pm k\hat{\mathbf{z}}$ only. This makes the determination of $\mathcal{M}_{(c_F)njm}^{(d)}$ matrix elements in the cavity frame relatively straightforward. For example, a short calculation gives spin-weighted Stokes parameters

$$\underline{s}^0(\mathbf{p}) = \frac{\langle U \rangle}{\epsilon} [\delta(\mathbf{p} - k\hat{\mathbf{z}}) + \delta(\mathbf{p} + k\hat{\mathbf{z}})] , \quad (13)$$

$$\underline{s}_{(\pm 2)}(\mathbf{p}) = -\frac{\langle U \rangle}{\epsilon} [\delta(\mathbf{p} - k\hat{\mathbf{z}})e^{\pm 2i\varphi} + \delta(\mathbf{p} + k\hat{\mathbf{z}})e^{\mp 2i\varphi}] , \quad (14)$$

in term of the energy $\langle U \rangle$ and the relative permittivity ϵ of the material filling the cavity, if present. This leads to

$$\begin{aligned} \mathcal{M}_{(c_F)njm}^{(d)\text{cav}} = & \frac{\omega^{d-4}N^{n-2}}{4\epsilon} \left[\frac{1}{4}(N^2 - 1)\sqrt{\frac{(j+2)!}{(j-2)!}} \left({}_{+2}Y_{jm}(\hat{\mathbf{z}})e^{2i\varphi} + {}_{-2}Y_{jm}(\hat{\mathbf{z}})e^{-2i\varphi} \right) \right. \\ & - \left((n - \frac{j(j+1)}{2})(N^2 - 1) + (d-2-n)(d-3-3n)N^2 + n(n-1)N^2 \right) {}_0Y_{jm}(\hat{\mathbf{z}}) \\ & \left. + (\hat{\mathbf{z}} \rightarrow -\hat{\mathbf{z}}, \varphi \rightarrow -\varphi) \right] \end{aligned} \quad (15)$$

where we let $N = k/\omega$ be the index of refraction of the media inside the cavity.

The advantage of the cavity frame is that the spin-weighted spherical harmonics take a simple form for propagation in the $\pm\hat{\mathbf{z}}$ direction. The only nonzero harmonics are those with $m = \mp s$ for propagation in the $\pm\hat{\mathbf{z}}$ direction. They are given by

$${}_sY_{j(-s)}(\hat{\mathbf{z}}) = \sqrt{\frac{2j+1}{4\pi}}(-1)^s e^{-is\varphi} , \quad (16)$$

$${}_sY_{js}(-\hat{\mathbf{z}}) = \sqrt{\frac{2j+1}{4\pi}}(-1)^{s+j} e^{is\varphi} , \quad (17)$$

provided $j \geq |s|$, as usual. Using these identities, we can write the cavity-frame matrices as

$$\mathcal{M}_{(c_F)njm}^{(d)\text{cav}} = \mathcal{U}_{nj}^{(d)}\delta_{m,0} + \mathcal{V}_{nj}^{(d)}\delta_{|m|,2} , \quad (18)$$

for even values of j . They are zero for odd values of j . The coefficients in the above expression are

$$\begin{aligned} \mathcal{U}_{nj}^{(d)} = & -\frac{\omega^{d-4}N^{n-2}}{2\epsilon} \sqrt{\frac{2j+1}{4\pi}} \left[\left(n - \frac{j(j+1)}{2} \right) (N^2 - 1) \right. \\ & \left. + (d-2-n)(d-3-3n)N^2 + n(n-1)N^2 \right] , \end{aligned} \quad (19)$$

$$\mathcal{V}_{nj}^{(d)} = \frac{\omega^{d-4}N^{n-2}(N^2 - 1)}{8\epsilon} \sqrt{\frac{(2j+1)(j+2)!}{4\pi(j-2)!}} . \quad (20)$$

These same numerical factors will appear again in the ring-resonator case discussed in the next section and generically determine the sensitivities of optical experiments to Lorentz violation.

Notice that the above results simplify dramatically in an empty cavity where $N = 1$. In particular, the $m = \pm 2$ matrix elements vanish and the only contribution is from the $m = 0$ terms. This implies invariance under rotations about the cavity axis, which means the result is independent of polarization. This stems from the fact that we are considering effects of nonbirefringent coefficients, which have a uniform effect on all polarizations. In matter, when $N \neq 1$, nonbirefringent coefficients can lead to birefringence [15]. Consequently, the introduction of media can lead to polarization dependence even when no polarization dependence results in the vacuum. In the present context, this is reflected in the possibility of azimuthal dependence from nonzero $\mathcal{M}_{(c_F)njm}^{(d)\text{cav}}$ matrix components for $m = \pm 2$.

Before we can apply the above result, we must transform the cavity-frame $\mathcal{M}_{(c_F)njm}^{(d)\text{cav}}$ matrix to the standard laboratory frame where z is vertical and the x axis is at an angle ϕ from south. In the spherical-harmonic basis, rotations take the form of Wigner matrices $D_{mm'}^{(j)}$ through the relation

$$\begin{aligned} \mathcal{M}_{(c_F)njm}^{(d)\text{lab}} = & \sum_{m'} \mathcal{M}_{(c_F)njm'}^{(d)\text{cav}} D_{m'm}^{(j)}(-\gamma, -\beta, -\alpha) \\ = & \sum_{m'} \mathcal{M}_{(c_F)njm'}^{(d)\text{cav}} e^{im'\gamma} e^{im\alpha} d_{m'm}^{(j)}(-\beta) , \end{aligned} \quad (21)$$

where α , β , and γ are the Euler angles relating the cavity and laboratory frames. The cavity frame is found by starting with the two frames aligned, then rotating the cavity frame by α about the z axis followed by a rotation

of β about the new y axis and a rotation of γ about the new z axis.

Most experiments involve cavities that lie in the horizontal plane. This is achieved by taking $\beta = 90^\circ$. Then α gives the angle between the cavity axis and the laboratory x axis and γ gives the angle of the polarization out of the horizontal plane. The result is then

$$\begin{aligned} \mathcal{M}_{(c_F)njm}^{(d)\text{lab}} &= \sum_{m'} \mathcal{M}_{(c_F)njm'}^{(d)\text{cav}} e^{im'\gamma} e^{im\alpha} d_{m'm}^{(j)}(-\frac{\pi}{2}) \\ &= \mathcal{U}_{nj}^{(d)} e^{im\alpha} d_{0m}^{(j)}(-\frac{\pi}{2}) \\ &\quad + \mathcal{V}_{nj}^{(d)} e^{im\alpha} e^{i2\gamma} d_{2m}^{(j)}(-\frac{\pi}{2}) \\ &\quad + \mathcal{V}_{nj}^{(d)} e^{im\alpha} e^{-i2\gamma} d_{-2m}^{(j)}(-\frac{\pi}{2}) . \end{aligned} \quad (22)$$

Again, only even values of j contribute in Fabry-Pérot cavities.

The above expression can now be used to find the modulation amplitudes in the beat frequency. Consider, for example, the two recent experiments in Refs. [7, 8]. Both experiments involve orthogonal Fabry-Pérot cavities. The cavities are empty, so there will be no polarization-dependent contribution from $\mathcal{V}_{nj}^{(d)}$. Taking one cavity along the laboratory x axis ($\alpha = 0$) and the other along the y axis ($\alpha = \pi/2$), variations in the beat frequency are controlled by

$$\Delta \mathcal{M}_{(c_F)njm}^{(d)\text{lab}} = \mathcal{U}_{nj}^{(d)} d_{0m}^{(j)}(-\frac{\pi}{2})(1 - i^m) . \quad (23)$$

Notice that this vanishes when m is a multiple of 4. This is because a 90° rotation about the vertical axis corresponds to interchanging the two cavities. Therefore, the beat frequency must change sign under a 90° rotation and is invariant under a 180° rotation. This implies that only harmonics with m equal to an even value not divisible by four can appear.

Both the experiments under consideration use Nd:YAG lasers as the radiation source ($\omega = 1.17$ eV) and lie at similar colatitudes, $\chi \simeq 38^\circ$. Consequently, both experiments are sensitive to nearly identical combinations of coefficients for Lorentz violation. These combinations are the modulation amplitudes from Eq. (8). They are given up to $d = 8$ in Table I. The table shows that we only expect variations at twice the turntable rate. While symmetry considerations prohibit turntable harmonics for odd values of m and multiples of four, higher-order variations with $m \geq 6$ can arise in general. Variations at six times the turntable frequency do arise from operators of dimension $d = 10$ and higher, for example. However, the absence of odd harmonics and those at multiples of four times the turntable rate is a generic feature of any experiment based on two identical crossed cavities lying in the horizontal plane. Choosing a relative angle other than the 90° or orienting one cavity out of the horizontal plane may provide additional sensitivity to Lorentz violation.

Comparing Table I to the microwave experiment in Ref. [10], we confirm the enhanced potential sensitivities arising from the ω^{d-4} dependence in the frequency shift.

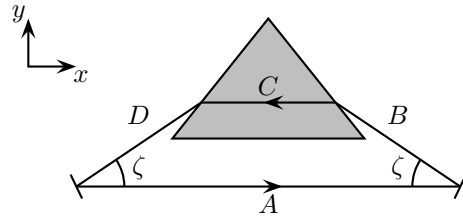


FIG. 1: Ring resonator composed of two mirrors and a prism with index of refraction N . The arms A , B , C , and D are of length L_A , L_B , L_C , and L_D , respectively. Refraction at the prism is at Brewster's angle. Polarization is linear in the plane of the ring. Arm A is oriented along the laboratory-frame x axis.

The table shows that the camouflage coefficients enter with a factor on the order of 10^{-18} GeV^2 for $d = 6$ and 10^{-36} GeV^4 for $d = 8$. Assuming dimensionless sensitivities to variations in the beat frequency on the order of 10^{-17} , we expect measurements of camouflage coefficients at the level of 10 GeV^{-2} for $d = 6$ and 10^{19} GeV^{-4} for $d = 8$. These sensitivities are many orders of magnitude beyond the current microwave bounds.

IV. RING RESONATOR

Ring resonators provide another example of an optical experiment sensitive to Lorentz violation. One advantage of a ring resonator is that it is not symmetric under parity. As a result, it can provide unsuppressed sensitivity to parity-odd coefficients for Lorentz violation. Here we will consider the resonator of Ref. [9] specifically, but other configurations are possible. The basic setup is shown in Fig. 1. Plane waves polarized in the plane of the oscillator propagate around the resonator. Resonant frequencies for the clockwise and counterclockwise modes are then compared and analyzed for signatures of Lorentz violation.

Much of the analysis of the ring resonator mirrors that of the Fabry-Pérot cavity. We begin by defining a beam frame where the wave propagates along the z axis and is polarized in the y direction. The beam is then given by the nonzero component $E_y(\mathbf{x}) = \mathcal{E}\rho(\mathbf{x})\exp ikz$, where ρ is the beam profile function. The smooth field is taken by extending the plane wave to infinity, $\underline{E}_y(\mathbf{x}) = \mathcal{E}\exp ikz$. Following the same steps as before, we find that the $\mathcal{M}_{(c_F)njm}^{(d)}$ matrix elements associated with radiation propagating in one direction in a given arm of the resonator is

$$\mathcal{M}_{(c_F)njm}^{(d)\text{arm}} = \mathcal{U}_{nj}^{(d)} \delta_{m,0} + \mathcal{V}_{nj}^{(d)} \delta_{|m|,2} , \quad (24)$$

where, in this case, j takes on any value satisfying $j \geq |m|$. The symmetries that prevented odd j values in the Fabry-Pérot case no longer apply, so all values of j can contribute, in principle. The $\mathcal{U}_{nj}^{(d)}$ and $\mathcal{V}_{nj}^{(d)}$ factors are given in Eqs. (19) and (20).

dimension	m	m'	$C_{mm'}^C$	$C_{mm'}^S$	$S_{mm'}^C$	$S_{mm'}^S$
$d = 4$	2	0	$-0.36 c_{(I)20}^{(4)}$	0	0	0
	2	1	$-0.75 \text{Re}[c_{(I)21}^{(4)}]$	$0.75 \text{Im}[c_{(I)21}^{(4)}]$	$0.95 \text{Im}[c_{(I)21}^{(4)}]$	$0.95 \text{Re}[c_{(I)21}^{(4)}]$
	2	2	$-1.3 \text{Re}[c_{(I)22}^{(4)}]$	$1.3 \text{Im}[c_{(I)22}^{(4)}]$	$1.2 \text{Im}[c_{(I)22}^{(4)}]$	$1.2 \text{Re}[c_{(I)22}^{(4)}]$
$d = 6$	2	0	$3.9 (\bar{c}_F^{(6)})_{220}^{(0E)}$	0	0	0
	2	1	$8.2 \text{Re}[(\bar{c}_F^{(6)})_{221}^{(0E)}]$	$-8.2 \text{Im}[(\bar{c}_F^{(6)})_{221}^{(0E)}]$	$-10 \text{Im}[(\bar{c}_F^{(6)})_{221}^{(0E)}]$	$-10 \text{Re}[(\bar{c}_F^{(6)})_{221}^{(0E)}]$
	2	2	$14 \text{Re}[(\bar{c}_F^{(6)})_{222}^{(0E)}]$	$-14 \text{Im}[(\bar{c}_F^{(6)})_{222}^{(0E)}]$	$-13 \text{Im}[(\bar{c}_F^{(6)})_{222}^{(0E)}]$	$-13 \text{Re}[(\bar{c}_F^{(6)})_{222}^{(0E)}]$
$d = 8$	2	0	$11 (\bar{c}_F^{(8)})_{420}^{(0E)}$ $-20 (\bar{c}_F^{(8)})_{440}^{(0E)}$			
	2	1	$22 \text{Re}[(\bar{c}_F^{(8)})_{421}^{(0E)}]$	$-22 \text{Im}[(\bar{c}_F^{(8)})_{421}^{(0E)}]$	$-29 \text{Im}[(\bar{c}_F^{(8)})_{421}^{(0E)}]$	$-29 \text{Re}[(\bar{c}_F^{(8)})_{421}^{(0E)}]$
			$-4.8 \text{Re}[(\bar{c}_F^{(8)})_{441}^{(0E)}]$	$+4.8 \text{Im}[(\bar{c}_F^{(8)})_{441}^{(0E)}]$	$+29 \text{Im}[(\bar{c}_F^{(8)})_{441}^{(0E)}]$	$+29 \text{Re}[(\bar{c}_F^{(8)})_{441}^{(0E)}]$
	2	2	$38 \text{Re}[(\bar{c}_F^{(8)})_{422}^{(0E)}]$	$-38 \text{Im}[(\bar{c}_F^{(8)})_{422}^{(0E)}]$	$-37 \text{Im}[(\bar{c}_F^{(8)})_{422}^{(0E)}]$	$-37 \text{Re}[(\bar{c}_F^{(8)})_{422}^{(0E)}]$
			$+0.53 \text{Re}[(\bar{c}_F^{(8)})_{442}^{(0E)}]$	$-0.53 \text{Im}[(\bar{c}_F^{(8)})_{442}^{(0E)}]$	$-10 \text{Im}[(\bar{c}_F^{(8)})_{442}^{(0E)}]$	$-10 \text{Re}[(\bar{c}_F^{(8)})_{442}^{(0E)}]$
	2	3	$23 \text{Re}[(\bar{c}_F^{(8)})_{443}^{(0E)}]$	$-23 \text{Im}[(\bar{c}_F^{(8)})_{443}^{(0E)}]$	$-20 \text{Im}[(\bar{c}_F^{(8)})_{443}^{(0E)}]$	$-20 \text{Re}[(\bar{c}_F^{(8)})_{443}^{(0E)}]$
	2	4	$-16 \text{Re}[(\bar{c}_F^{(8)})_{444}^{(0E)}]$	$16 \text{Im}[(\bar{c}_F^{(8)})_{444}^{(0E)}]$	$16 \text{Im}[(\bar{c}_F^{(8)})_{444}^{(0E)}]$	$16 \text{Re}[(\bar{c}_F^{(8)})_{444}^{(0E)}]$

TABLE I: Nonzero modulation amplitudes for the Fabry-Pérot cavities in Refs. [7, 8]. Camouflage coefficients up to dimension $d = 8$ are included. The numbers m and m' give the harmonics of the turntable rotation frequency and sidereal frequency, respectively. The dimension-6 amplitudes are in units of 10^{-18} GeV^2 . The dimension-8 amplitudes are in units of 10^{-36} GeV^4 .

The above calculation gives the contribution from a single arm. The total $\mathcal{M}_{(c_F)njm}^{(d)}$ matrix for a given mode is the energy-weighted average of all the arms. To find the average, we must first rotate the single arm result $\mathcal{M}_{(c_F)njm}^{(d) \text{ arm}}$ to get the proper orientation in the laboratory frame.

Consider the counterclockwise mode propagating around the ring in Fig. 1. For arms A , B , and D we take $N = 1$, which gives zero $\mathcal{V}_{nj}^{(d)}$. The $\mathcal{M}_{(c_F)njm}^{(d)}$ matrix for arm A is then obtained by a $\beta = 90^\circ$ rotation about the y axis, giving a beam propagating in the laboratory-frame x direction. For B , the $\beta = 90^\circ$ rotation is preceded by a $\alpha = 180^\circ - \zeta$ rotation about the z axis. Similarly, the matrix for C is given by rotation angles $\alpha = 180^\circ$ and $\beta = 90^\circ$, and arm D is found using $\alpha = 180^\circ + \zeta$ and $\beta = 90^\circ$. The resulting laboratory-frame matrix elements can be written as

$$\mathcal{M}_{(c_F)njm}^{(d)A} = \mathcal{U}_{nj}^{(d)A} d_{0m}^{(j)}(-\frac{\pi}{2}), \quad (25)$$

$$\mathcal{M}_{(c_F)njm}^{(d)B} = \mathcal{U}_{nj}^{(d)B} (-1)^m e^{-im\zeta} d_{0m}^{(j)}(-\frac{\pi}{2}), \quad (26)$$

$$\begin{aligned} \mathcal{M}_{(c_F)njm}^{(d)C} &= \mathcal{U}_{nj}^{(d)C} (-1)^m d_{0m}^{(j)}(-\frac{\pi}{2}) \\ &+ \mathcal{V}_{nj}^{(d)C} (-1)^m \left(d_{2m}^{(j)}(-\frac{\pi}{2}) + d_{(-2)m}^{(j)}(-\frac{\pi}{2}) \right), \quad (27) \end{aligned}$$

$$\mathcal{M}_{(c_F)njm}^{(d)D} = \mathcal{U}_{nj}^{(d)D} (-1)^m e^{im\zeta} d_{0m}^{(j)}(-\frac{\pi}{2}), \quad (28)$$

where $\mathcal{U}_{nj}^{(d)A} = \mathcal{U}_{nj}^{(d)B} = \mathcal{U}_{nj}^{(d)D}$ is obtained by taking $N = 1$ in Eq. (19), while $\mathcal{U}_{nj}^{(d)C}$, $\mathcal{V}_{nj}^{(d)C}$ are found using the index of refraction for the prism $N = N_{\text{prism}}$ in (19) and (20).

We next take the energy-weighted average of the four arms to get the total laboratory-frame $\mathcal{M}_{(c_F)njm}^{(d) \text{ lab}}$ matrix. Assuming perfect reflections at the mirrors and Brewster's-angle refraction at the prism, the power of the beam is the same in all four arms. We may then write the power $P = \lambda v = \lambda/N = \text{constant}$, where λ is the energy per length of the beam. The energy in a particular arm is $\langle U \rangle_{\text{arm}} = \lambda L = PNL$. This implies that the energy is proportional to the optical length NL . So, the energy fraction in a given arm is the same as the fraction of the total optical length attributed to that arm. The laboratory-frame matrix for the ring resonator is then given by

$$\begin{aligned} \mathcal{M}_{(c_F)njm}^{(d) \text{ lab}} &= \frac{L_A}{L_{\text{opt}}} \mathcal{M}_{(c_F)njm}^{(d)A} + \frac{L_B}{L_{\text{opt}}} \mathcal{M}_{(c_F)njm}^{(d)B} \\ &+ \frac{NL_C}{L_{\text{opt}}} \mathcal{M}_{(c_F)njm}^{(d)C} + \frac{L_D}{L_{\text{opt}}} \mathcal{M}_{(c_F)njm}^{(d)D}, \quad (29) \end{aligned}$$

dimension	m	m'	$C_{mm'}^C$	$C_{mm'}^S$	$S_{mm'}^C$	$S_{mm'}^S$
$d = 6$	1	0	$0.22 (\bar{c}_F^{(6)})_{110}^{(0E)}$	0	0	0
	1	1	$-0.20 \text{Re}[(\bar{c}_F^{(6)})_{111}^{(0E)}]$	$0.20 \text{Im}[(\bar{c}_F^{(6)})_{111}^{(0E)}]$	$-0.37 \text{Im}[(\bar{c}_F^{(6)})_{111}^{(0E)}]$	$-0.37 \text{Re}[(\bar{c}_F^{(6)})_{111}^{(0E)}]$
$d = 8$	1	0	$-0.61 (\bar{c}_F^{(8)})_{110}^{(0E)}$ $+6.5 (\bar{c}_F^{(8)})_{310}^{(0E)}$ $-1.5 (\bar{c}_F^{(8)})_{330}^{(0E)}$	0	0	0
	1	1	$0.54 \text{Re}[(\bar{c}_F^{(8)})_{111}^{(0E)}]$	$-0.54 \text{Im}[(\bar{c}_F^{(8)})_{111}^{(0E)}]$	$1.0 \text{Im}[(\bar{c}_F^{(8)})_{111}^{(0E)}]$	$1.0 \text{Re}[(\bar{c}_F^{(8)})_{111}^{(0E)}]$
			$-5.8 \text{Re}[(\bar{c}_F^{(8)})_{311}^{(0E)}]$	$+5.8 \text{Im}[(\bar{c}_F^{(8)})_{311}^{(0E)}]$	$-11 \text{Im}[(\bar{c}_F^{(8)})_{311}^{(0E)}]$	$-11 \text{Re}[(\bar{c}_F^{(8)})_{311}^{(0E)}]$
			$-9.2 \text{Re}[(\bar{c}_F^{(8)})_{331}^{(0E)}]$	$+9.2 \text{Im}[(\bar{c}_F^{(8)})_{331}^{(0E)}]$	$+1.0 \text{Im}[(\bar{c}_F^{(8)})_{331}^{(0E)}]$	$+1.0 \text{Re}[(\bar{c}_F^{(8)})_{331}^{(0E)}]$
	1	2	$-1.1 \text{Re}[(\bar{c}_F^{(8)})_{332}^{(0E)}]$	$1.1 \text{Im}[(\bar{c}_F^{(8)})_{332}^{(0E)}]$	$7.2 \text{Im}[(\bar{c}_F^{(8)})_{332}^{(0E)}]$	$7.2 \text{Re}[(\bar{c}_F^{(8)})_{332}^{(0E)}]$
	1	3	$3.8 \text{Re}[(\bar{c}_F^{(8)})_{333}^{(0E)}]$	$-3.8 \text{Im}[(\bar{c}_F^{(8)})_{333}^{(0E)}]$	$7.1 \text{Im}[(\bar{c}_F^{(8)})_{333}^{(0E)}]$	$7.1 \text{Re}[(\bar{c}_F^{(8)})_{333}^{(0E)}]$
	3	0	$2.5 \text{Re}[(\bar{c}_F^{(8)})_{330}^{(0E)}]$	0	0	0
	3	1	$-2.7 \text{Re}[(\bar{c}_F^{(8)})_{331}^{(0E)}]$	$2.7 \text{Im}[(\bar{c}_F^{(8)})_{331}^{(0E)}]$	$-5.0 \text{Im}[(\bar{c}_F^{(8)})_{331}^{(0E)}]$	$-5.0 \text{Re}[(\bar{c}_F^{(8)})_{331}^{(0E)}]$
	3	2	$4.8 \text{Re}[(\bar{c}_F^{(8)})_{332}^{(0E)}]$	$-4.8 \text{Im}[(\bar{c}_F^{(8)})_{332}^{(0E)}]$	$4.0 \text{Im}[(\bar{c}_F^{(8)})_{332}^{(0E)}]$	$4.0 \text{Re}[(\bar{c}_F^{(8)})_{332}^{(0E)}]$
	3	3	$-3.2 \text{Re}[(\bar{c}_F^{(8)})_{333}^{(0E)}]$	$3.2 \text{Im}[(\bar{c}_F^{(8)})_{333}^{(0E)}]$	$-3.3 \text{Im}[(\bar{c}_F^{(8)})_{333}^{(0E)}]$	$-3.3 \text{Re}[(\bar{c}_F^{(8)})_{333}^{(0E)}]$

TABLE II: Nonzero modulation amplitudes for the ring resonator in Ref. [9]. Camouflage coefficients up to dimension $d = 8$ are included. The numbers m and m' give the harmonics of the turntable rotation frequency and sidereal frequency, respectively. The dimension-6 amplitudes are in units of 10^{-18} GeV². The dimension-8 amplitudes are in units of 10^{-36} GeV⁴.

where $L_{\text{opt}} = L_A + L_B + NL_C + L_D$ is the total optical path length.

Unlike the Fabry-Pérot example, where we compare identical modes in two different cavities, in this case we compare two different modes in the same resonator. The above calculation yields the frequency shift for the counterclockwise-propagating mode. To get $\mathcal{M}_{(c_F)njm}^{(d)}$ for the clockwise mode, we note that a reversal in propagation in each arm is achieved through a 180° rotation about the laboratory-frame z axis. This implies that the clockwise mode can be found by multiplying the above result by $e^{im\pi} = (-1)^m$. We then get

$$\Delta\mathcal{M}_{(c_F)njm}^{(d)\text{lab}} = (1 - (-1)^m)\mathcal{M}_{(c_F)njm}^{(d)\text{lab}}. \quad (30)$$

Notice that this vanishes for even values of m . A 180° rotation about the vertical effectively interchanges the two modes, changing the sign of the beat frequency. As a result, no even harmonics of the turntable frequency can appear. A parity transformation also interchanges the two modes, changing the sign of the beat frequency. Consequently, only parity-odd coefficients for Lorentz violation should affect the beat frequency. In the current context, this corresponds to odd values of j .

The advantage of the ring resonator over most other

cavity experiments is its sensitivity to parity-odd coefficients. In order to demonstrate this sensitivity explicitly, we consider the parameters for the experiment in Ref. [9]. The dimensions are $L_A = 34.9$ mm, $L_B = L_D = 11.1$ mm, and $L_C = 14.1$ mm and the index of refraction of the prism is $N_{\text{prism}} = 1.44$ [28]. Again, the photon energy is approximately $\omega = 1.17$ eV. The colatitude for this experiment is $\chi = 122^\circ$. The resulting modulation amplitudes up to dimension $d = 8$ are given in Table II. Sensitivity to $j = 1$ and $j = 3$ coefficients is achieved, as expected. Note, however, that the mSME $d = 4$ coefficients do not appear.

The absence of $d = 4$ coefficients can be understood by focusing on the nonbirefringent parity-odd mSME terms. There are a total of three coefficients in this limit, which have previously been characterized using an antisymmetric constant 3×3 matrix $\tilde{\kappa}_{o+}^{(4)}$ [19]. The frequency shift due to these coefficients can be written as

$$\frac{\delta\nu}{\nu} = -\frac{1}{2\langle U \rangle} \epsilon^{jkl} (\tilde{\kappa}_{o+}^{(4)})^{kl} \int d^3x \mu \langle S^j \rangle, \quad (31)$$

where $\langle \mathbf{S} \rangle = \frac{1}{2} \text{Re} \mathbf{E}^* \times \mathbf{H}$ is the time-averaged Poynting vector, and μ is the permeability of the media. For a constant permeability, the frequency shift is proportional

coef.	F.-P.	ring	P-even	P-odd	iso.
$c_{(I)jm}^{(4)}$	5	0	5	3	1
$(\bar{c}_F^{(6)})_{njm}^{(0E)}$	5	3	5	3	2
$(\bar{c}_F^{(8)})_{njm}^{(0E)}$	13	12	19	13	3

TABLE III: Numbers of combinations of $d = 4, 6, 8$ camouflage coefficients accessible to the existing experiments discussed in this work. The second column gives the number of parity-even coefficients accessible to the Fabry-Pérot experiments of Ref. [7, 8]. The third column gives the number of parity-odd coefficients for the ring resonator of Ref. [9]. For comparison, the next three columns give the number of parity-even anisotropic, parity-odd anisotropic, and isotropic camouflage coefficients.

to the Poynting vector averaged over the volume of the resonator, which vanishes for a closed system. Consequently, a lossless resonator cannot provide sensitivity to these coefficients unless media with different permeabilities are included. We can show this explicitly in the ring resonator. The Poynting vector in one arm can be written as $\langle \mathbf{S} \rangle = P\mathbf{L}/V$, where P is the power, \mathbf{L} is the beam length vector, and V is the beam volume. The frequency shift then becomes

$$\frac{\delta\nu}{\nu} = \frac{1}{2} \epsilon^{jkl} (\tilde{\kappa}_{o+}^{(4)})^{kl} \frac{\sum_a \mu_a L_a^j}{L_{\text{opt}}}, \quad (32)$$

where we sum over the arms, $a = A, B, C, D$. This is proportional to the vector sum of the \mathbf{L}_a vectors in the event that the permeability μ is the same in all arms. The sum vanishes for a closed path.

V. DISCUSSION

The results obtained in the two examples given here are easily generalized to other optical experiments with linear polarization. Assuming the resonator modes can be decomposed into the superposition of plane waves, we can use Eq. (24) to get the contribution from each wave. We then use Wigner matrices, as in Eq. (21), to rotate the result for each component wave, giving it the correct orientation in the laboratory. Taking the energy-weighted

average of the waves, we arrive at the laboratory-frame $\mathcal{M}_{(c_F)njm}^{(d)}$ matrix for the resonator.

As an example, a Fabry-Pérot cavity aligned with the laboratory x axis can be treated as two plane waves at angles $\alpha = 0, \pi$. A cavity aligned with the y axis has $\alpha = \frac{1}{2}\pi, \frac{3}{2}\pi$. For index of refraction $N = 1$, the difference is then

$$\begin{aligned} \Delta\mathcal{M}_{(c_F)njm}^{(d)\text{lab}} &= \frac{1}{2}(1 + e^{im\pi} - e^{im\pi/2} - e^{im3\pi/2}) \\ &\quad \times \mathcal{U}_{nj}^{(d)} d_{0m}^{(j)}(-\frac{\pi}{2}) \\ &= \frac{1}{2}(1 - i^m)(1 + (-1)^m) \mathcal{U}_{nj}^{(d)} d_{0m}^{(j)}(-\frac{\pi}{2}), \end{aligned} \quad (33)$$

which vanishes unless m is an even integer not divisible by four. Using this and the property that $d_{0m}^{(j)}(-\frac{\pi}{2})$ vanishes unless j and m are either both even or both odd, we arrive at the same result obtained in Sec. III for crossed Fabry-Pérot cavities.

The above methods can be applied to new optical experiments utilizing different configurations. These may provide sensitivity to different combinations of coefficients for Lorentz violation. The results of this work demonstrate that, while a large portion of the coefficient space is accessible to the two types of experiment discussed here, other experiments are needed to fully constrain the coefficients up to $d = 8$. Table III summarizes the results. A given Fabry-Pérot experiment based on orthogonal cavities can measure twenty-three of the twenty-nine anisotropic parity-even camouflage coefficients. A single ring resonator can test all but four of the nineteen parity-odd coefficients.

Similar numbers are expected for higher dimensions, $d = 10, 12, \dots$, which are easily included in an analysis. One could also consider the larger class of nonbirefringent coefficients $(c_F^{(d)})_{njm}^{(0E)}$, which include dispersive effects. Only a few bounds from astrophysical dispersion exist at present. So cavity experiments currently offer an opportunity for an indirect search for this unconventional feature at interesting sensitivities. Future analyses could also take advantage of boost effects to probe the isotropic coefficients. These tests would see suppressions in sensitivity of roughly $\beta^2 \sim 10^{-8}$ in a parity-even experiment and $\beta \sim 10^{-4}$ in a parity-odd experiment. Nonetheless, they may offer the best opportunity for searches for these elusive forms of Lorentz violation.

-
- [1] V.A. Kostelecký and S. Samuel, Phys. Rev. D **39**, 683 (1989); V.A. Kostelecký and R. Potting, Nucl. Phys. B **359**, 545 (1991); Phys. Rev. D **51**, 3923 (1995).
[2] V.A. Kostelecký and N. Russell, Rev. Mod. Phys. **83**, 11 (2011).
[3] A.A. Michelson and E.W. Morley, Am. J. Sci. **34**, 333 (1887); Phil. Mag. **24**, 449 (1887).
[4] J. Lipa *et al.*, Phys. Rev. Lett. **90**, 060403 (2003); P. Wolf *et al.*, Gen. Rel. Grav. **36**, 2352 (2004); P. Wolf *et*

- al.*, Phys. Rev. D **70**, 051902 (2004); P.L. Stanwix *et al.*, Phys. Rev. Lett. **95**, 040404 (2005); P.L. Stanwix *et al.*, Phys. Rev. D **74**, 081101 (2006); M.A. Hohensee *et al.*, Phys. Rev. D **82**, 076001 (2010).
[5] H. Müller *et al.*, Phys. Rev. Lett. **91**, 020401 (2003); S. Herrmann *et al.*, Phys. Rev. Lett. **95**, 150401 (2005); P. Antonini *et al.*, Phys. Rev. A **71**, 050101 (2005); **72**, 066102 (2005); M.E. Tobar, P. Wolf, and P.L. Stanwix, Phys. Rev. A **72**, 066101 (2005).

- [6] H. Müller *et al.*, Phys. Rev. D **67**, 056006 (2003); H. Müller *et al.*, Phys. Rev. D **68**, 116006 (2003); H. Müller, Phys. Rev. D **71**, 045004 (2005); H. Müller *et al.*, Phys. Rev. Lett. **99**, 050401 (2007); M. Mewes, Phys. Rev. D **78**, 096008 (2008).
- [7] Ch. Eisele, A.Yu. Nevsky, and S. Schiller, Phys. Rev. Lett. **103**, 090401 (2009).
- [8] S. Herrmann *et al.*, Phys. Rev. D **80**, 105011 (2009).
- [9] F.N. Baynes, A.N. Luiten, and M.E. Tobar, Phys. Rev. D **84**, 081101 (2011).
- [10] S.R. Parker *et al.*, Phys. Rev. Lett. **106**, 180401 (2011).
- [11] D. Colladay and V.A. Kostelecký, Phys. Rev. D **55**, 6760 (1997); **58**, 116002 (1998).
- [12] V.A. Kostelecký, Phys. Rev. D **69**, 105009 (2004); Q.G. Bailey and V.A. Kostelecký, Phys. Rev. D **74**, 045001 (2006); V.A. Kostelecký, N. Russell, and J.D. Tasson, Phys. Rev. Lett. **100**, 111102 (2008); Q.G. Bailey, Phys. Rev. D **80**, 044004 (2009); **82**, 065012 (2010); V.A. Kostelecký and J.D. Tasson, Phys. Rev. Lett. **102**, 010402 (2009); Phys. Rev. D **83**, 016013 (2011); R. Tso and Q.G. Bailey, Phys. Rev. D **84**, 085025 (2011).
- [13] J.B.R. Battat, J.F. Chandler, and C.W. Stubbs, Phys. Rev. Lett. **99**, 241103 (2007); H. Müller *et al.*, Phys. Rev. Lett. **100**, 031101 (2008); K.-Y. Chung *et al.*, Phys. Rev. D **80**, 016002 (2009); D. Bennett, V. Skavysh, and J. Long, in V.A. Kostelecký ed., *CPT and Lorentz Symmetry V*, World Scientific, Singapore, 2011; M.A. Hohensee *et al.*, Phys. Rev. Lett. **106**, 151102 (2011).
- [14] V.A. Kostelecký and M. Mewes, Ap. J. Lett. **689**, L1 (2008).
- [15] V.A. Kostelecký and M. Mewes, Phys. Rev. D **80**, 015020 (2009).
- [16] V. Vasileiou, arXiv:1008.2913; F.W. Stecker, Astropart. Phys. **35**, 95 (2011).
- [17] C.M. Reyes, Phys. Rev. D **82**, 125036 (2010); B. Altschul, Phys. Rev. D **83**, 056012 (2011); B. Agostini *et al.*, Phys. Lett. B **708**, 212 (2012); M. Cambiaso, R. Lehnert, and R. Potting, arXiv:1201.3045.
- [18] J.S. Diaz and V.A. Kostelecký, Phys. Lett. B **700**, 25 (2011); Phys. Rev. D **85**, 016013 (2012); V.A. Kostelecký and M. Mewes, arXiv:1112.6395.
- [19] V.A. Kostelecký and M. Mewes, Phys. Rev. D **66**, 056005 (2002).
- [20] S.M. Carroll, G.B. Field, and R. Jackiw, Phys. Rev. D **41**, 1231 (1990); V.A. Kostelecký and M. Mewes, Phys. Rev. Lett. **87**, 251304 (2001); **97**, 140401 (2006); **99**, 011601 (2007); T. Kahniashvili, R. Durrer, and Y. Maravin, Phys. Rev. D **78**, 123009 (2008); E.Y.S. Wu *et al.*, Phys. Rev. Lett. **102**, 161302 (2009); Z. Xiao and B.-Q. Ma, Phys. Rev. D **80**, 116005 (2009); G. Gubitosi *et al.*, JCAP **08**, 021 (2009); E. Komatsu *et al.*, Ap. J. Suppl. **192**, 18 (2011); Q. Exirifard, Phys. Lett. B **699**, 1 (2011).
- [21] M.E. Tobar *et al.*, Phys. Rev. D **71**, 025004 (2005); M.E. Tobar *et al.*, Phys. Rev. D **80**, 125024 (2009).
- [22] Q. Exirifard, arXiv:1010.2057.
- [23] M. Mewes and A. Petroff, Phys. Rev. D **75**, 056002 (2007).
- [24] Q.G. Bailey and V.A. Kostelecký, Phys. Rev. D **70**, 076006 (2004); A. Kobakhidze and B.H.J. McKellar, Phys. Rev. D **76**, 093004 (2007); R. Casana, M.M. Ferreira, and C.E.H. Santos, Phys. Rev. D **78**, 105014 (2008).
- [25] M.A. Hohensee *et al.*, Phys. Rev. D **80**, 036010 (2009); Phys. Rev. Lett. **102**, 170402 (2009); B. Altschul, Phys. Rev. D **80**, 091901 (2009); J.-P. Bocquet *et al.*, Phys. Rev. Lett. **104**, 241601 (2010).
- [26] R. Lehnert and R. Potting, Phys. Rev. Lett. **93**, 110402 (2004); Phys. Rev. D **70**, 125010 (2004); C. Kaufhold and F.R. Klinkhamer, Nucl. Phys. **734**, 1 (2006); Phys. Rev. D **76**, 025024 (2007); B. Altschul, Phys. Rev. Lett. **98**, 041603 (2007); Phys. Rev. D **75**, 105003 (2007); Nucl. Phys. B **796**, 262 (2008); F.R. Klinkhamer and M. Risse, Phys. Rev. D **77**, 016002 (2008); **77**, 117901 (2008); F.R. Klinkhamer and M. Schreck, Phys. Rev. D **78**, 085026 (2008); F.R. Klinkhamer, Phys. Rev. D **82**, 105024 (2010).
- [27] V.A. Kostelecký and A.G.M. Pickering, Phys. Rev. Lett. **91**, 031801 (2003); B. Altschul, Phys. Rev. D **72**, 085003 (2005); C.D. Carone, M. Sher, and M. Vanderhaeghen, Phys. Rev. D **74**, 077901 (2006); J.P. Cotter and B.T.H. Varcoe, arXiv:physics/0603111; S. Reinhardt *et al.*, Nature Phys. **3**, 861 (2007); M. Hohensee *et al.*, Phys. Rev. D **75**, 049902(E) (2007); J.M. Fonseca, A.H. Gomes, and W.A. Moura-Melo, Phys. Lett. B **671**, 280 (2009); L. Campanelli and P. Cea, Phys. Lett. B **675**, 155 (2009); A.H. Gomes *et al.*, JHEP **1005**, 104 (2010).
- [28] M.E. Tobar (private communication).